SLAC-PUB-7051
January, 1996

BEAM-BEAM EFFECTS and GENERALIZED LUMINOSITY

J.E. SPENCER*
Stanford Linear Accelerator Center
Stanford University, Stanford, CA 94309

The assumption is made that before an NLC is approved, a prototype will be necessary that demonstrates the feasibility of a general purpose linear collider capable of $\vec{e}^{\pm}\vec{e}^{\pm}$, $\vec{\gamma}\vec{e}^{\pm}$ and $\vec{\gamma}\vec{\gamma}$ incident channels. At an upgraded SLC, such channels could provide new physics over a range of energies upwards of a few GeV. Effects that limit the luminosity of a GLC are discussed together with their possible mitigations. The expected luminosities in the different channels are then predicted in a consistent way for $\sqrt{s}_{ee}$= 0.5 TeV.

1. Introduction

Because a recent workshop[1] concentrated on $\vec{\gamma}\vec{\gamma}$ collisions, it is useful to look at $\vec{e}^{-}\vec{e}^{-}$ because electron beams are used to produce all the others. With the possible exception of $e\gamma$, this channel has received the least attention[2] even though it was the first one that was used to produce colliding beam physics. $e\gamma$ and $e^{-}e^{-}$ collisions provide the possibility of doing new physics at SLC energies[3] long before any NLC (or GLC) could be built. Further, given an NLC with a second interaction region, one can expect that these channels could come on-line earlier than $e^{+}e^{-}$. Because the $e^{+}e^{-}$ option is reasonably well understood, I concentrate on the other channels since positrons are an unnecessary complication for a single linac such as the SLC. Thus, our primary goal is to optimize the $\vec{e}^{-}\vec{e}^{-}$ luminosity ($\equiv\mathcal{L}_{ee}$) for a GLC. However, because the beam dynamics of the $e^{+}e^{-}$ channel have been well verified at the SLC and studied for the NLC, we use this channel to estimate the achievable luminosities in the other channels.

Because it is always possible to increase $\mathcal{L}$ if we are allowed to increase the beam power P_b (see below), we will talk about relative luminosity rather than absolute and assume that our current understanding of what is achievable for the NLC in the $e^{+}e^{-}$ channel sets the scale for the others. Thus, we begin by discussing our current expectations[4] for $e^{+}e^{-}$ at 0.5 and 1.0 TeV. Although many of the characteristic parameters for different designs such as the NLC or TESLA differ by more than an order of magnitude, the luminosities are all comparable. Next we generalize the luminosity in terms of channel efficiencies and beam-beam disruption effects. The influence of these effects in the different channels are then calculated and the results summarized in tables for different channel configurations.

Presented at (e-e- 1995):Proceedings of the Electron-Electron Linear Collider Workshop, Santa Cruz, CA, September 4-5, 1995

*Work supported by the U.S. Department of Energy under contract DE-AC03-76SF00515.

2. Achievable e^- Beams

We make the conservative assumption that any practically achievable e^- beams for the NLC e^+e^- designs are also available for e^-e^-. Table I gives some configurations at two energies with those labelled 'A' currently preferred. $\mathcal{L}_{e^\pm}$ and $\mathcal{L}_{e^-e^-}$ are the predicted channel luminosities for these parameters whereas $\mathcal{L}_{Compton}$ and $\mathcal{L}_{\gamma\gamma}$ are secondary to the e^+e^- channel. $\mathcal{L}_{\gamma\gamma}$ is rather large because it includes contributions from real and virtual photons and the beamsstrahlung parameter Υ is fairly large. Υ is an important measure of the QED and QCD backgrounds expressed in terms of $\gamma\gamma\to e^+e^-$ pairs and minijets ($\gamma\gamma\to$X + anything). N_p/N_e is the ratio of outgoing positrons per incident electron for energies E_p>10 MeV and angles $\theta\geq$10 mr. Other parameters are described in more detail below. Because there is still debate on how to calculate the hadronic 'backgrounds' in terms of the various possible quark and gluon contributions at these energies, they are not listed. There is interesting physics available here if it could be measured but an upgraded SLC[5] would seem to be a better place to find new hadrons, quark molecules or glueballs.[3,6]

Table I: Beam-Beam Effects for e^+e^- at E_{cm}=0.5, 1.0 TeV and $\gamma\epsilon_x = 5\times10^{-6}$ m. Quantities enclosed in (...) are calculated rather than simulations. See text for *s.

$\sqrt{s}_{\rm NLC}$ [GeV]	500	500A	1000	1000A
$f_{\rm rep}$[Hz]	180	180	120	120
n_B	90	90	75	90
$\gamma\epsilon_y[10^{-8}m]$	5	8	5	10
$N_B[10^{10}]$	0.65	0.65	1.1	0.95
σ_x^*/σ_y^*[nm]	319.7/3.2	285.9/4.52	360/2.3	226.1/3.57
$\sigma_z[\mu m]$	100	100	100	125
β_x^*/β_y^*[mm]	10/0.1	8/0.125	25/0.1	10/0.125
$\mathcal{L}_G[10^{34}{\rm cm}^{-2}{\rm sec}^{-1}]$	0.53	0.42	1.05	0.96
D_x/D_y	0.073/7.3	0.090/5.70	0.049/7.60	0.132/8.33
$\theta_D=\theta_{x,max}[\mu$rad]	233	257	175	238
Υ	0.09	0.10	0.27	0.30
$H_D\equiv\mathcal{L}/\mathcal{L}_G$	1.37	1.42	1.30	1.36
$\mathcal{L}_{e^\pm}[10^{34}{\rm cm}^{-2}{\rm sec}^{-1}]$	0.73	0.60	1.37	1.30
$\langle s\rangle/s_{\rm NLC}$		0.972		0.913
$\langle E_\circ - E_{in}\rangle/E_{in}$	0.019	0.032	0.0711	0.103
$\delta_B\equiv E_\circ^{rms}/E_{in}$	0.042	0.065	0.120	0.143
$\mathcal{L}_{100}/\mathcal{L}_{e^\pm}$	0.441	0.376(0.405)	0.305(0.323)	0.195(0.218)
$\mathcal{L}_{90}/\mathcal{L}_{e^\pm}$	(0.83)	(0.80)	(0.84)	(0.75)
N_γ/N_e	0.88	0.98	1.213	1.67
$\langle E_\gamma\rangle/E_\circ$	0.027	0.033	0.059	0.062
$N_p/N_e[10^{-7}]$*		2.41		4.95
$\langle E_p\rangle$ [MeV]		39.0		39.0
$\mathcal{L}_{Compton}$		0.23		0.80
$\mathcal{L}_{\gamma\gamma}[10^{34}{\rm cm}^{-2}{\rm sec}^{-1}]$		0.10		0.56
$\mathcal{L}_{e^-e^-}$		0.23		0.45

Beyond the standard, two-body invariants there are the dimensionless, classical and quantal strong-field invariants: Υ involving a particle's Compton wavelength and η involving the photon's wavelength:

$$\eta \;=\frac{e}{m}\Big[-\frac{(F_{\mu\nu}p_1^{\nu})^2}{(p_1k_1)^2}\Big]^{\frac{1}{2}} \;\rightarrow\; \frac{e\sqrt{\langle A_\mu A^\mu\rangle}}{m}=\frac{e\langle\mathcal{E}_{Lab}\rangle}{m}\lambda\!\!\!^{-} = \;\Upsilon\frac{m^2}{2\omega_1\epsilon_1}$$

where $\hbar$=c=1 and the arrow implies head-on collisions. η=1 (Υ=1) corresponds to an energy gain of one electron mass over one photon (Compton) reduced wavelength. $\eta\rightarrow\infty$, $\omega\rightarrow 0$ is the static field limit. Although one writes the fields as if they were constant, their variation within the beams provide observable ponderomotive effects and their external variations (e.g. via the intensity or wavelength of the laser used to produce the photon beams) provide low-order 'knobs'. When the $\mathcal{E}$ and $\mathcal{B}$ fields are equal and orthogonal as in a plane wave, pure field invariants such as ${F_{\mu\nu}}^2=\mathcal{E}^2$-$\mathcal{B}^2$ don't give us such knobs but normalizing them provides a measure of the 'strength' of any field. Thus, when the boosted field $\mathcal{E}^*$ of a counterpropagating beam in the average rest frame of the other compared to the Schwinger critical field $\mathcal{E}_c\equiv m^2/e$ approaches unity ($\Upsilon\rightarrow 1$) we expect the pair channel to couple strongly.

In Table I, $\Upsilon\leq 0.3$ is a typical limit set to control beamsstrahlung intensity (e.g. the pair backgrounds) but there is no consensus and for the two energies labelled 'A' in Table I, the only comparable parameters are H_D and $R\equiv\sigma_x^*/\sigma_y^*$, the beam's unperturbed aspect ratio at the IP. While many of the parameters in Table I such as Υ, D (the disruption) and δ_B (the final rms energy spread due to beamsstrahlung) all go inversely as some power of 1+R, there are also wide variations in R between competing designs for e^+e^-. Because one can increase (decrease) $\mathcal{L}_{e^\pm}$ ($\mathcal{L}_{e^-e^-}$) by increasing these parameters at the cost of increasing the detector backgrounds and occupancy we will first discuss the luminosity in a more general way.

3. The Generalized Luminosity $\mathcal{L}$

From the expression for $\mathcal{L}$ for gaussian incident bunches, we want to first maximize the particles in a single bunch N_B and minimize the undisrupted, rms spot sizes $\sigma_{x,y}^*$, then optimize the number of bunches in a train n_B and finally the RF rep-rate f_T (the number of bunch trains/s) in a self-consistent way:

$$\mathcal{L} \;=\; \frac{f_T n_B N_B^2 H_D}{4\pi\sigma_x^*\sigma_y^*}\zeta \;\rightarrow\; \frac{f_T n_B N_B^2\gamma H_D}{4\pi\epsilon_n\beta^*}\;\zeta \;=\frac{f_T n_B N_B^2\gamma}{4\pi\widehat{\sigma}^2}\;\zeta \;\propto\; \frac{P_b}{\widehat{\sigma}^2}\Big(\frac{\widehat{N}_B^2}{N_B}\Big)$$

where the arrow simplifies the expression to round beams (R≡1). The dimensionless parameter H_D is the luminosity 'enhancement' defined in terms of the geometric luminosity as $\mathcal{L}/\mathcal{L}_G$ when the efficiency factor ζ=1. H_D includes disruption effects from the beam-beam interaction and, together with ζ, will be discussed later. P_b is the electron beam power and ϵ_n is the invariant emittance. β^* is the magneto-optical 'depth of field' at the IP equivalent to the Rayleigh range Z_R for lasers.

While one would like to put all particles into a single bunch with n_B=f_T=1, this is impractical even for individual RF pulses because of emittance, energy spread and beamsstrahlung implications. However, because the bandwidth of the control

system and the stability of the accelerator and its various subsystems relates more to the RF rep-rate f_T than to the bunch number n_B, a practical solution appears to be multibunch trains to partition the total charge/pulse into a more continuous flow during each RF pulse and to have a reasonably high RF rep-rate. Thus, most of the current designs propose to accelerate several bunches per RF pulse with a lower N_B than for the SLC to improve energy (or wall-plug) efficiency and average luminosity[5]. For an RF system efficiency >30 %, the required wall plug power is ≈100 and 200 MW for the two energies labelled 'A' in Table I.

The undisrupted rms spot size σ^* at a round focus, in terms of the beam energy E_e, is

$$\sigma^* = \left(\frac{\epsilon_n \beta^*}{\gamma}\right)^{\frac{1}{2}} = \frac{1}{\sqrt{E_{e\,(\mathrm{GeV})}}}\ \mu\mathrm{m} \quad \text{for} \quad \epsilon_n = 2\mu\mathrm{m},\ \beta^* = 1\mathrm{mm}\,.$$

With such characteristics in a 'second generation' collider we expect a luminosity:

$$\mathcal{L} \approx E_{e\,(\mathrm{GeV})} \cdot H_D \zeta \cdot 10^{31}\ \mathrm{cm}^{-2}\mathrm{s}^{-1} \quad \text{for} \quad f_T = 120, n_B = 100, N_B = 10^{10}.$$

$\mathcal{L}$ varies linearly with incident energy if the other parameters are independent of energy. To get $\mathcal{L} \geq 5 \cdot 10^{32}$ we need an incident electron energy $E_e \geq 50$ GeV – the nominal energy of the SLC. We also need to calculate $\mathrm{H_D}$ and ζ. A luminosity $\mathcal{L} \geq 10^{32}$ would be enough to search for the lowest mass Higgs[7] or selectron or to test point-like predictions for the $\tilde{e}_R$, W or Z as well as to explicate the light meson spectrum at the SLC.[3,6]

Discounting any stability problems for e^-e^-, the efficiency factor ζ should be better for e^-e^- than for e^+e^-[5] and it can be improved by increasing both n_B and f_T. However, to get more high quality charge through the linac that maintains ϵ_n for every bunch in a train of n_B bunches we can not arbitrarily increase N_B due to the bunch's interaction with its surroundings and their back reaction on it or succeeding bunches via effects such as wake fields. A dramatic example of this occurs at the IP during the beam-beam interaction where beamsstrahlung (notice that it takes two beams for this to occur) increases both the longitudinal and transverse emittances.

Similarly, decreasing the geometric spot sizes induces similar problems and also worsens the effects of any given bunch charge N_B. Maxwell's equations limit our ability to simultaneously minimize σ_x^* and σ_y^* or β_x^* and β_y^* with normal lenses but a charge neutralizing plasma or ion beam could make e^-e^- approach e^+e^- luminosity. Nevertheless, for any N_B and σ's, we can always increase $\mathcal{L}$ by increasing the beam power P_b via f_T and/or n_B. Likewise, to obtain the same nonresonant event rate at twice the energy costs us a factor of 2^4 more power for an equivalent storage ring when both types of collider are operating at their respective beam-beam limits.

Because we specifically avoided labels on the luminosity $\mathcal{L}$ such as $\mathcal{L}_{ee}$ or on the number of 'particles' in a bunch N_B we can include in ζ the different channel dependent efficiencies such as the probability of converting $e \to \gamma$ (just as for $e^- \to e^+$) because we get $\mathcal{L}_{e\gamma}$ or $\mathcal{L}_{\gamma\gamma}$ from $\mathcal{L}_{ee}$ by folding it with the Compton conversion process. We will calculate this contribution to ζ in the strong field regime where pairs can be produced in the cross channel reaction to the (nonlinear) Compton process. Together with $\mathrm{H_D}$ this gives the generalized luminosity $\mathcal{L}$ for a GLC.

4. Conversion and Interaction Region Physics

The first colliding beam physics was done at Stanford in the early '60's with e^-e^- and the idea of a $\gamma\gamma$ collider has been discussed at SLAC since the late '70s. Before the design or approval of the SLC project the subject of a second IR was raised for such channels. Later, the possibility of real γ channels in conjunction with storage rings was considered and most recently as a luminosity upgrade for the SLC within the context of a second generation linear collider and its extension to a GLC.

An important part of the nonlinear QED experiment E144[9] on the FFTB line at SLAC is based on such possibilities. In particular, that experiment is an essential 'proof-of-principle' for such new incident channels based on using real photons to provide a general linear collider[0]. The laser wavelength, intensity and the classical, strong-field, intensity parameter η that are being used in that experiment are the same as assumed here because these parameters are ideally matched to an NLC with 250 GeV electron beams.

4.1. *Basic Constraints and Assumptions*

We note that for multibunch operation (n_B>1), we need to introduce crossing angles at the IR and design the FF quadrupoles to minimize the effects of the outgoing, disrupted beam on the incoming. This decreases ζ so that we need to introduce variable, crab-crossing cavities[8,4] that rotate the beams to the proper orientation at the IP or CP (the $e\gamma$ conversion point) to restore ζ. We will show that such cavities are required for all channels but otherwise ignore them.

Because preceding bunches may perturb the effective emittance, energy and spread of every following bunch, multibunch beam loading and phase compensation is required to determine the best distribution of charge over each RF pulse. Because this has been done for the e^+e^- channel on the NLC we will assume that the latest configurations and beam parameters for that channel are available for e^-e^- and $\gamma\gamma$. Although these are not optimal for either e^-e^- or $\gamma\gamma$ they provide a good starting point so the main problem is to compute H_D and ζ for the new channels within the framework given in Table I. Then, because these configurations and beam characteristics are not optimized for the other channels, we will vary them over reasonable limits to improve H_D and ζ to find the achievable luminosities in all channels.

If there is a second IP, one can argue that e^-e^- should be done in conjunction with the $\gamma\gamma$ channel. Ignoring detector considerations, these channels are better to combine than e^+e^- and e^-e^- because: 1) there should be minimal hysteresis effects, 2) the deviations from the e^+e^- channel that one would like to implement based on our calculations such as variations in the bunch charge N_B and/or the bunch length σ_z turn out to be common to both channels but go in opposite directions for e^-e^- and $\gamma\gamma$ so that we require bipolar 'knobs' for their implementation and 3) this combination would also appear to allow a better overall uptime efficiency by separating e^-e^- from e^+ production with its added damping requirements.

4.2. *Machine Configurations and Beam Parameters*

The configurations and beam parameters such as β^*, N_B and D for two energies are given in Table I. Other configurations based on these such as LC'95 or SC'95 for $\gamma\gamma$ or e^-e^- are straightforward variants and are described where they are used. The variations on these standard configurations at either energy in Table I are given in Tables II-III where the main results are summarized. As an example, 'Case A' emittance implies $\gamma\epsilon_{x,y}$ in the second or fourth columns of Table I. Parameters such as the number of electrons (or positrons) per bunch apply to both beams unless otherwise stated. Machine parameters that are not discussed such as l^*, the distance from the IP to the first quad, are the same as for 'A' in Table I (see Ref. 4).

All calculations such as those with ABEL91[0] and our variants of it were checked by analytic calculations wherever practicable (e.g. see the discussion in Section 11.7 of Ref. 4). In particular, we have archived files of the outgoing disrupted electrons, photons and pairs for all of these configurations for use in design studies of the detector and dump line as well as for other possible uses such as secondary beams and dump line experiments.[4]

4.3. *The Beam-Beam Interaction*

The typical emission angle for high energy radiative processes such as incoherent bremsstrahlung is $\theta_r \approx 1/\gamma \approx 1$ μrad at 500 GeV. As the photon energy decreases, the angles begin to grow compared to θ_r as does the interaction volume of the electron. When an electron interacts with the collective field of the other bunch it sees transverse electric and magnetic fields that are nearly equal ($eN_B/\sigma_z\sigma_r$). Within a given bunch these cancel but can easily bend a counterpropagating particle by angles significantly greater than θ_r. The resulting radiation, similar to synchrotron radiation, is called beamsstrahlung.

4.3.1. *Disruption Effects*

A characteristic angle for the full-energy, primary, disrupted particles that we will call the disruption angle is then simply[0]:

$$\theta_D \equiv \frac{2N_B r_e}{\gamma(\sigma_x + \sigma_y)} = \frac{D_{x,y}\sigma_{x,y}}{\sigma_z}$$

where $\sigma_{x,y}/\sigma_z$ is sometimes called the diagonal angle θ_d and equals θ_D when $D_{x,y}$=1. When the crossing angle $\theta_c > \theta_d$ one needs crab-crossing cavities. The disruption is defined as σ_z/f where f is the effective focal length provided by one beam on the other (for e^+e^- it is focusing and for e^-e^- it is defocusing). Table I gives a few characteristic examples. Clearly, D (and θ_D) are related to the beam-beam tune shift that limits the luminosity of storage rings. Typically, in the e^+e^- channel, the maximum disruption angle is in the horizontal with $\theta_{x,max}=\theta_D$ because the disruption parameter in the vertical is so large that one gets over focusing or a thick lens effect which gives an oscillatory motion whereas the focusing over the length of the beam in x is weaker but cumulative or more like a thin lens. The rms angles are $\sigma_{x',y'}$=0.55 θ_D. For e^-e^- the situation reverses and the vertical disruption angle dominates – more in line with the naive expectation.

An important difference for IPs involving γ_s is the degraded electron beam from the conversion process. The outgoing beam is highly disrupted but also necessarily includes a significant fraction of electrons at full incident energy. The lowest order Compton edge (electrons) is:

$$E_{edge} = E_e \cdot y \approx E_e/5.5 \quad \text{where} \quad y = \frac{1}{1+x}$$

and

$$x = 2p_e k_L/(p_e p_e) \rightarrow 4E_e\omega_L/m^2 = 0.0153 E_{e(\mathrm{GeV})}\omega_{L(\mathrm{eV})}.$$

For E_e=250 GeV and the Nd:glass fundamental assumed here this gives E_{edge}=45 GeV. Because $D_{x,y}$ varies inversely with electron energy, it follows that:

$$D_{edge} = (1+x)D_{x,y} \approx 5.5 \cdot D_{x,y} \qquad \text{(lowest order)}.$$

This implies that the detector fields can have a serious influence on the outgoing beam characteristics. Thus, if detector simulations imply an unacceptable background from this or too high occupancy from the full energy $\mathcal{L}_{ee}$ this procedure has to be iterated for a consistent solution.

Our solution to this problem has been to introduce a small offset between the incoming beam centroids at the IP since this gives strong bending fields between like charged beams with little loss of $\gamma\gamma$ luminosity. For undisrupted beams ($H_D \approx 1$), the luminosity varies exponentially with the square of the separation or offset between the beams so that

$$\zeta_{ND}(\Delta_{x,y}) = \frac{\mathcal{L}_G(\Delta_{x,y})}{\mathcal{L}_G(0)} = e^{-\Delta^2_{x,y}/2\Sigma^2_{x,y}}$$

where $\Delta_{x,y}$ is the transverse offset of the two beams and Σ_y (Σ_x) is the quadrature sum of the rms vertical (horizontal) beam sizes for the two colliding beams. A good test of the beam-beam calculations is to compare to these predictions for small disruptions. We see that D influences both luminosity and backgrounds and that it can also be used to reduce the detector occupancy.

4.3.2. *Beam-Beam Results*

Because of space limitations, only a few results are discussed in any detail but the more important calculations are summarized in Tables I-III. Figure 1 shows some representative beam-beam simulations for $\gamma\gamma$, e^-e^- and e^+e^- that illustrate the effects of disruption for the same beam and machine parameters when E_e=250 GeV. The lower part of the figure shows the disrupted bunch distribution when it is centered at the IP. Some nonreal rays that are offset from the beam centroid transversely as well as longitudinally at the head and tail of a bunch are also included to show the effects of disruption when it is operative. The enhancement factor H is the integral of the distributions shown in the top half of Fig. 1. Because the γ beams are produced upstream of the IP (at the Compton conversion point CP) there is no conventional disruption and the photons collide at the IP with the same beam sizes as the originating electron beam would have had when not in collision when we make the separation between the CP and IP sufficiently small.[3,6]

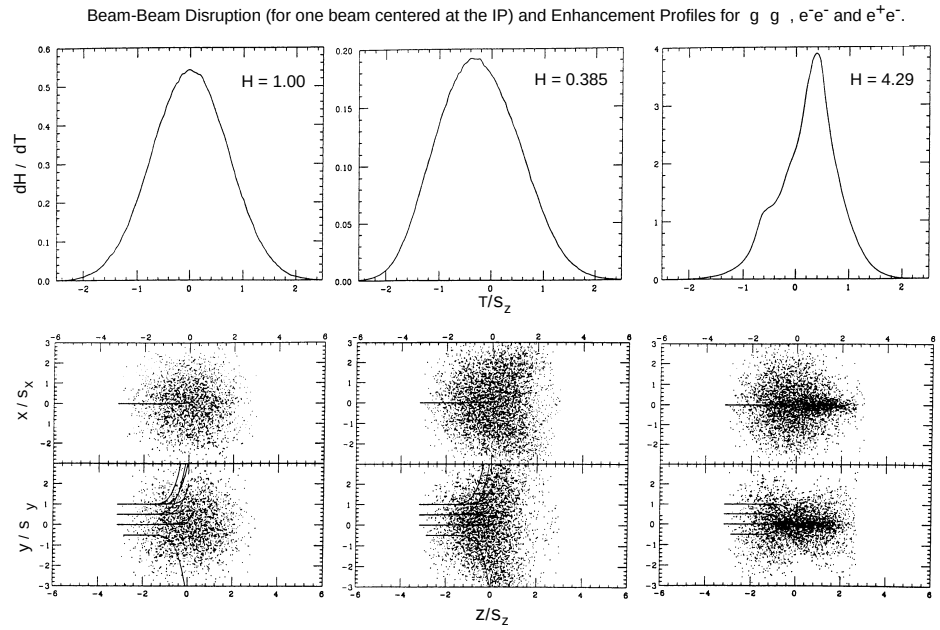

Fig. 1: Predicted distributions for LC'95A parameters in the different channels.

The distribution of 'enhancement' demonstrates the lensing action in two ways. Noting that the γ beams have no charge, we see that the distribution of the peak luminosity is pushed forward or backward depending on the relative sign of the beam charge and the distribution is also widened or narrowed depending on this sign (the sign of the lens). When there is significant disruption ($H_D \neq 1$), there is also a fore-aft asymmetry. Focusing modulation and disruption is especially evident in Fig. 1 for e^+e^- demonstrating the importance of realistic (trigaussian) distributions for the input bunches and the strong perturbation on shape, geometric σ_s and ϵ_n that may occur in both transverse and longitudinal directions. While H_D was not listed in Tables II or III due to its relation with ζ, it can be calculated for the cases in Fig. 1 from the luminosities $\mathcal{L}$ listed in Table III for LC'95A which is the latest $\gamma\gamma$ configuration consistent with the e^+e^- channel configuration 'A' in Table I.

Table II: Luminosity calculations for LC'95.[a] 'ND' means no disruption.[b] δx, δy & $\theta_{c,x}$ are centroid offsets and crossing angles. $D_{x,y}$ is for full energy.

N_B	RF	n_B	$D_{x,y}$	Luminosity $[10^{34}]$				Parameters
$[10^{10}]$	1/s		Disruption	Head-On	Offset	Slope	Both	δx,y and $\theta_{c,x}$
0.70	180	90	(ND)	1.25	0.98	0.09	0.07	$1\sigma_y$/20 mr
0.70	180	90	1.47,14.7	0.41	0.11			$1\sigma_y$
1.05	120	90	(ND)	1.88	1.47	0.14	0.11	$1\sigma_y$/20 mr
1.05	120	90	2.20,22.0	0.49	0.13			$1\sigma_y$

[a] $\epsilon_{n,x}=5\cdot10^{-6}$ m, $\epsilon_{n,y}=0.01\epsilon_{n,x}$, $\beta_x^*=\beta_y^*=0.5$ mm & $\sigma_z=100$ μ for the LC'95 configuration.
[b] Statistics imply an accuracy of $\pm1\%$ but no radiative or pair effects were included.

For the LC'95 configuration in Table II, the progenitor of LC'95A, we see that a $1\sigma_y$ offset reduces $\mathcal{L}_{\gamma\gamma}(\sigma_y)$ to $0.78\mathcal{L}_{\gamma\gamma}(0)$ as expected analytically. H_D for e^-e^- is reduced to 0.33 by the smaller emittance and larger bunch charge. Because $\mathcal{L}$ falls from 125 to 9×10^{32} for a crossing angle θ_c=20 mrad,[4] it is clear that crab cavities are needed for all channels (see next section). Also, anticipating results from Fig. 2, the unconverted, full energy electrons contribute a relative e^-e^- luminosity of only $0.11/0.98[\zeta_\gamma/\epsilon_1^e]^2$=0.62% for a $1\sigma_y$ offset where $\zeta_\gamma \equiv \epsilon_{1-10}^{\gamma}$=1.255. This is clearly preferable to that without an offset and can be improved by increasing the bunch charge to increase the electron disruption. Another method, suggested by Balakin and Sery[1], that in principle might also work is to offset only the head of each bunch. One can (and must) then introduce larger beam offsets without losing as much $\gamma\gamma$ luminosity. However, for stable operation, this needs too high an RF frequency to be practical (related to a fraction of the bunch length) and therefore wasn't calculated. A sample calculation of ζ for LC'95A is discussed next.

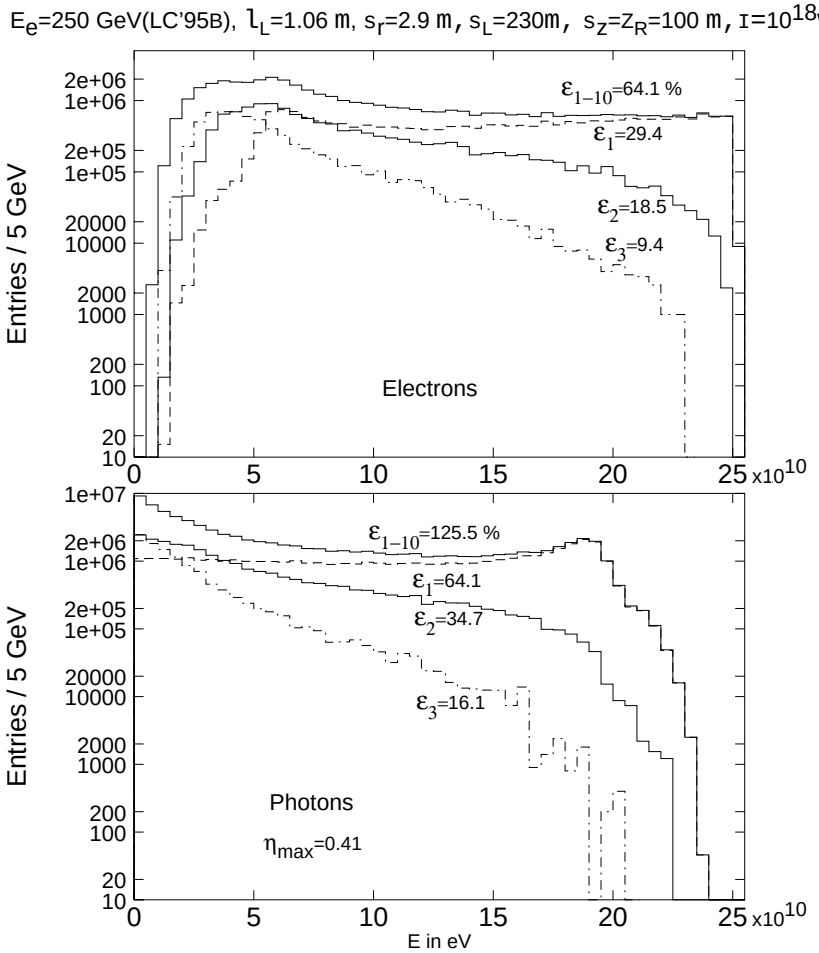

Fig. 2: Predicted spectrum of electrons and photons for Case A in Tables I and III.

4.4. *Calculations for the CP and IP*

A necessary part of this study is the efficient conversion of the electron beams at the Compton conversion point CP – located here at l_c^*=5 mm upstream from the γ IP. This location allows the higher energy photons to collide with the same spot size that the undisrupted electrons would have had. Using 'LC95A' for e^-e^- in Table III, one finds σ_x/σ_y=71.5/9.04 nm at the IP while $\sigma_x(l_c^*)/\sigma_y(l_c^*)$=0.72/0.09$\mu$m which is still much less than the diffraction limited laser spot size.

Table III: Predicted luminosity for various incident channels & configurations[a] 'ND' indicates no disruption effects.[b] $D_{x,y}$ is for the full energy incident beams.

Case E_B=250 GeV	N_B [10^{10}]	RF 1/s	n_B	$D_{x,y}$ Disruption	$\mathcal{L}$ [10^{34}]	Characteristics ϵ_n,σ_z,n_γ,H_D,...
(e^-e^-)						
LC'95	0.70	180	90	(ND)	1.25	σ_z=100 μ
LC'95	0.70	180	90	1.47,14.7	0.41	
'LC'95'	1.05	120	90	(ND)	1.88	
'LC'95'	1.05	120	90	2.20,22.0	0.49	
(e^+e^-)						
LC'95A	0.65	180	90	(ND)	0.83	$\epsilon_{n,y}\equiv 8\cdot 10^{-8}$m
LC'95A	0.65	180	90	1.30,10.3	3.56	All-n_γ>5n_e
LC'95A	0.65	180	90	1.30,10.3	3.18	No Radiative
Case A[c]	0.65	180	90	(ND)	0.42	
Case A[c]	0.65	180	90	0.09,5.70	0.60	All-$n_\gamma\approx n_e$
(e^-e^-)						
Case A[c]	0.65	180	90	0.09,5.70	0.23	H_D=0.55
LC'95A	0.65	180	90	1.30,10.3	0.32	σ_z=100 μ
LC'95A	0.65	180	90	0.65,5.14	0.44	σ_z=50 μ
LC'95A	0.65	180	90	1.95,15.4	0.26	σ_z=150 μ
LC'95A	0.50	180	117	(ND)	0.66	σ_z=100 μ
LC'95A	0.50	180	117	1.00,7.91	0.28	
SC'95A[d]	0.65	180	90	(ND)	0.22	$\epsilon_n\equiv 2.5\cdot 10^{-6}$m
SC'95A	0.65	180	90	1.46,1.46	0.11	σ_z=100 μ
SC'95A	0.65	360	90	1.46,1.46	0.23	$$
SC'95A	1.05	120	90	(ND)	0.37	
SC'95A	1.05	120	90	2.37,2.37	0.14	
SC'95A	0.50	180	117	(ND)	0.17	
SC'95A	0.50	180	117	1.13,1.13	0.10	H_D=0.59

[a] $\epsilon_{n,x}=5\cdot 10^{-6}$ m, $\epsilon_{n,y}=0.01\epsilon_{n,x}$ and $\beta_x^*=\beta_y^*$=0.5 mm for LC'95.
[b] Statistics imply an accuracy of ±1% here but without radiative or pair effects.
[c] $\epsilon_{n,x}=5\cdot 10^{-6}$m, $\epsilon_{n,y}=8\cdot 10^{-8}$m and β_x^*=8 mm, β_y^*=0.125 mm (Case A – Table I).
[d] $\epsilon_{n,x}=\epsilon_{n,y}=2.5\cdot 10^{-6}$ m and $\beta_x^*=\beta_y^*$=0.5 mm.

To get the actually expected luminosities from Tables II or III, we now need to calculate the $e\to\gamma$ conversion efficiency as well as that for producing a given γ bandwidth. Fig. 2 shows a representative calculation for the $e\vec{\gamma}$ conversion process for circularly polarized photons on unpolarized electrons with YACC a CAIN/ABEL

variant. The laser parameters are given in the figure where the various subscripts on the efficiencies indicate the order of the multiple scattering. A fully polarized laser is assumed but no polarization was assumed for the electrons because the luminosity is a strong function of electron polarization which is expected to be ≤80%. The corresponding $e\gamma$ and $\gamma\gamma$ luminosities can therefore be considered as conservative for any reasonably limited γ bandwidth. Absolute numbers of electrons or photons can be obtained in Fig. 2 by multiplying by 100.

Figs. 1-2 show the highly nonlinear character of the beam-beam interactions in all channels. This is especially evident in Fig. 2 for the photon spectrum above the conventional Compton threshold near 200 GeV. Because of high order multiple scattering and multiphoton conversion there is also intensity far below the electron Compton edge near 46 GeV as seen by comparing the different distributions in the figures with the curves labelled ϵ_1. Including such effects we find:

$$E_{min} = E_{in}/(1 + ns/m^{*2}) \; ; \quad s = 2E_{in}E_\gamma(1 + cos\theta_c^*) \approx 4E_\gamma(\text{eV})E_{in}(\text{TeV}) \; [\text{MeV}^2]$$

where θ_c^* is the laser's crossing angle with the electron beam at the CP and m^* is the effective mass[9,0] in the laser field given by $m\sqrt{1+\eta^2}$. From this we expect E_{min}/E_{in}≈2.5% with a corresponding disruption:

$$D_{max} = (1 + ns/m^{*2})D_{x,y} = (1 + \eta^2 + ns/m^2)D_{x,y}/(1 + \eta^2) \; .$$

This implies a crossing angle that is about seven times larger than linear but this is still less than half of the machine crossing angle of θ_c=20 mr that was assumed. From Fig. 2, the intensity at these energies is predominantly due to multiple scattering rather than single-step multiphoton processes. The detector fields can seriously influence the incoming and outgoing beam characteristics (detector backgrounds) with larger crossing angles or lower energies than assumed here.

For the calculations in Fig. 2 we find a conversion efficiency

$$\zeta = \mathcal{L}_{e\gamma}/\mathcal{L}_G = \epsilon_1^\gamma \zeta_{E_\gamma} = 0.641 \cdot 0.153 = 0.098 \quad \text{for} \quad \langle E_\gamma \rangle = 188 \pm 12\text{GeV}$$

with ζ_{E_γ} the fractional number of photons within the specified energy bandwidth. Notice that the "central" photon energy is displaced downward from the usual Compton (or Klein-Nishina) edge for two reasons. The less obvious one is that there is an effective mass increase of the electron in the strong laser field due to multiphoton absorption.[0]

5. Achievable Luminosities for Different Incident Channels

While e^+e^- has the natural advantage of a pinch enhancement, e^-e^- is cleaner than the other channels because it is severely limited by charge and lepton number conservation. In contrast, the $\gamma\gamma$ channel has the worst backgrounds since QCD enters at the same order as the standard electroweak processes. [0] The $e\gamma$ channel has a unique $\sqrt{s}$ advantage that is especially attractive for an upgraded SLC because it allows the possibility of studying the W and its anomalous couplings, e^* and the selectron $\tilde{e}_R$ at currently achievable energies.

The combination of these different incident channels and the polarizations they allow provides unprecedented control of quantum numbers such as the channel spin. Such "knobs" allow one to do multiple, independent experiments for a broad range of final states as well as to optimize them in various ways such as eliminating other final states that represent strong backgrounds.

The expected luminosities for a nominal 250×250 GeV GLC ($\sqrt{s}_{ee}$≡500 GeV) based on the assumptions and corresponding calculations above are summarized in Table IV. Thus, $\langle s_{\pm}\rangle/s_{ee}$=0.972 for e^+e^- with an effective rms energy spread in each beam of $\delta_{\rm E}$=3.5%. Similarly, for the γ beam(s) we have $\langle s_{\gamma\gamma}\rangle/s_{ee}$=0.752 with $\delta_{\rm E}$=6.4% in each beam. As mentioned above, this explains the "less-than" sign in Table IV which is based on a mass shift in the strong laser conversion field. We note that if we were to use polarized electrons that we can more than double the $e\gamma$ and quadruple the $\gamma\gamma$ luminosities (depending on the degree of electron polarization) or if we increase the γ energy spread, we can almost double the e^+e^- luminosity in the $e\gamma$ channel if we also reduce the separation distance between the CP and IP sufficiently to insure that all photon energies overlap the electrons at the IP.

Table IV: Achievable luminosities for a GLC with 250 GeV unpolarized, incident electrons. The luminosity integral is over one Snowmass year.

Incident Channel	$\mathcal{L}$ $[10^{33}/\mathrm{cm}^2\ \mathrm{s}]$	$\int \mathcal{L}\mathrm{dt}$ $[\mathrm{fmb}^{-1}]$	Threshold Energy	Comments
e^+e^-	6	60	$\sqrt{s_{ee}}$	Pinch Enhanced
e^-e^-	3	30	$\sqrt{s_{ee}}$	AntiPinch/Polarization
$e^{\pm}\gamma$	≥1	≥10	$< 0.91\sqrt{s_{ee}}$	$\sqrt{s}$ Discovery Advantage
γ-γ	≥0.1	≥1	$< 0.83\sqrt{s_{ee}}$	Backgrounds

6. Conclusions

A general expression for the luminosity was discussed that is consistent with all of the beam species that are likely to be of interest for a linear collider. As with other expressions,[0] it depends on essentially three quantities: the average, primary beam power; the average rms bunch size at the IP when the beams are in collision; and the average number of particles in a bunch that can be collided with that size. Because we argued that the luminosity can always be increased by increasing the beam power, we chose a well-studied, characteristic e^+e^- beam configuration that is considered achievable for the NLC to calculate a consistent set of luminosities for the other channels. This luminosity $\mathcal{L}_{\pm}$ is consistent with predictions for other machines such as the JLC and TESLA and the other luminosities in Table IV appear conservative in several respects as discussed.

Nevertheless, there are serious concerns for the inherent dynamical instabilities in the e^-e^- channels and the general question of backgrounds. These could be resolved by an SLC upgrade that could also provide interesting physics.

A number of peripheral observations were made. For example, tailoring the charge density could improve luminosity and charge sweeping produced by beam offsets in the γ channels. Simple variations in the bunch charges and bunch lengths are also effective and appear practical. Crab cavities are required for all channels. Such factors together with magnetic hysteresis provide a justification for combining the $\gamma\gamma$ and e^-e^- channels at a common IP. This is facilitated by the fact that an electron sweeping magnet for the γ channels does not appear necessary by using the field generated by the beam offsets (a 4 nm separation and typical bunch currents of 4 kA gives a 200 T sweeping field between bunches). However, detector simulations need to be the final arbiter between such schemes.

SLAC experiment E144 has verified some of the nonlinear QED effects associated with the strong laser fields required and can also test the conversion efficiency calculations[0]. Other difficult problems such as synchronization of the laser and electron pulses have also necessarily been addressed in this study which is ongoing.

A major distinction between e^-e^- and the other channels is that one wants a reasonably large disruption for pinch enhancement in e^+e^- and for dispersal of the low energy Compton electrons in the γ channels to reduce their unwanted luminosity whereas such increases in disruption reduce the luminosity in the e^-e^- channel. This is why we explored smaller disruptions $D_x \leq 1$ in Table III and suggested some disruption compensation schemes for e^-e^-.

Thus, because we expect that $H_D < 1$ for the e^-e^- channel, it is clear that without some form of field compensation scheme for e^-e^- we can expect $\mathcal{L}_{e^\pm} > \mathcal{L}_{e^-e^-}$ even with different optics configurations and beam parameters. This is another justification for a second IP at the NLC because it could then use the same lasers required for producing γ beams to produce a charge compensating plasma that could make e^-e^- comparable to e^+e^-. However, focused ion beams, that would avoid producing the high plasma densities, appear preferable for this if they can be produced.

Of course, the most important justification for IP2 is the combined physics reach of the e^-e^-, $e\gamma$ and $\gamma\gamma$ channels that exceeds that for e^+e^- as demonstrated by the various contributions to this conference. Further, because the e^-e^- channel is simpler to implement, it could run sooner with $\mathcal{L}_{e^-e^-} > 10^{33}$ by using the Santa Cruz'95 configuration for round beams in Table III. This would avoid the inevitable overhead costs of producing flat, low emittance beams of e^+(or e^-).

Acknowledgements

The author would like to thank Clem Heusch and Nora Rogers for a very productive and enjoyable workshop. He would also like to thank Nora, Anatoly Spitkovsky and Achim Weidemann for their various input as well as the other participants for many stimulating discussions. This work was supported by the U.S. Department of Energy under contract DE-AC03-76SF00515.

References

1. Workshop on Gamma-Gamma Colliders, S. Chattopadhyay and A.M. Sessler, Ed's., Berkeley, CA, March 28-31, 1994. Proc's in Nucl. Instrum. Methods **A355**(1995)1.
2. Clemens A. Heusch, e^-e^- physics at an e^-e^- collider, ibidem.
3. J.E. Spencer, Uses of a Prototype NLC/GLC, ibidem.
4. ZDR Workbook, Current version of the NLC Proposal dated 10/16/95.
5. J.E. Spencer, The SLC as a Second Generation Linear Collider, Proc's: 16th IEEE Part. Accel. Conf. and Int'l. Conf. on High Energy Accel's., R. Siemann, Ed., Dallas, TX, May 1-5, 1995.
6. D.A. Bauer, D.L. Borden, D.J. Miller and J.E. Spencer, The Use of a Prototype Next Linear Collider for $\gamma\gamma$ and $e\gamma$ collisions, SLAC-PUB-5816, 1992.
7. D.L. Borden, D.A. Bauer, and D.O. Caldwell, Physics Posibilities at a Photon Linear Collider, SLAC-PUB-5715, 1992.
8. R.B. Palmer, Prospects for High Energy e^+e^- Linear Colliders, Ann. Rev. Nucl. Sci. **40**(1990)529.
9. J.G. Heinrich, C. Lu, K.T. McDonald (Princeton U.), C.Bamber, A.C. Melissinos, D. Meyerhofer, Y. Semertzidis (Rochester U.), P. Chen, J.E. Spencer (SLAC), R.B. Palmer (SLAC,BNL), Proposal for a Study of QED at Critical Field Strength in Intense Laser High-Energy Electron Collisions at the Stanford Linear Accelerator, SLAC Proposal E144, Oct. 1991.
10. J.E. Spencer, Test of QED Using a Laser at the SLAC Final Focus Test Beam, Proc. IXth Int'l. Workshop on Photon-Photon Collisions, D.O. Caldwell and H.P. Paar, Ed's., UC, San Diego, March 22-26, 1992.
11. K. Yokoya, ABEL, Analysis of Beam-Beam Effects in Linear Colliders, Nucl. Instrum. Methods **A251**(1986)1 and T. Tauchi et al. Part. Accel. **41**(1993)29.
12. Robert Hollebeek, Disruption Limits for Linear Colliders, NIM **184**(1981)333.
13. S.J. Brodsky and P.M. Zerwas, High Energy Photon-Photon Collisions, SLAC-PUB-6571, 1994 and Workshop on Gamma-Gamma Colliders, ibidem.
14. Robert H. Siemann, Linear Colliders: The Last Ten Years and the Next Ten, SLAC-PUB-6417, 1994.
15. C. Bula, K.T. McDonald, E.J. Prebys (Princeton), C.Bamber, S. Boege, T. Koffas, T. Kotseroglou, A.C. Melissinos, D.D. Meyerhofer and W. Ragg (Rochester), D.L. Burke, R.C. Field, G. Horton-Smith, A.C. Odian, J.E. Spencer, D. Walz (SLAC), S.C. Berridge, W.M. Bugg, K. Shmakov and A.W. Weidemann (Tennessee), Observation of Nonlinear Effects in Compton Scattering, Submitted to Phys. Rev. Letters.